# The Surface of Mars: The View from the Viking 2 Lander

Abstract. *Viking 2 lander began imaging the surface of Mars at Utopia Planitia on 3 September 1976. The surface is a boulder-strewn reddish desert cut by troughs that probably form a polygonal network. A plateau can be seen to the east of the spacecraft, which for the most probable lander location is approximately the direction of a tongue of ejecta from the crater Mie. Boulders at the lander 2 site are generally more vesicular than those near lander 1. Fines at both lander sites appear to be very fine-grained and to be bound in a duricrust. The pinkish color of the sky, similar to that observed at the lander 1 site, indicates suspension of surface material. However, the atmospheric optical depth is less than that at the lander 1 site. After dissipation of a cloud of dust stirred during landing, no changes other than those stemming from sampling activities have been detected in the landscape. No signs of large organisms are apparent at either landing site.*

On 3 September 1976, at 09:48:58 after local Mars midnight, the Viking 2 spacecraft landed on the surface of Mars in the Utopia Planitia region (47.89°N, 225.86°W). The side of the triangular spacecraft on which the two cameras are mounted faces approximately north. When the cameras are pointed in a direction normal to the spacecraft front, the viewing direction is 29.13° clockwise from north. The lander is tilted 8.2° down in a direction 277.7° clockwise from north. Considering the fact that the terrain is generally flat but littered with boulders, it is possible that one edge of the lander frame is perched on a large boulder.

*General geological setting*. The Utopia Planitia region is part of the vast plains that occupy much of the northern hemisphere of Mars. Viking orbiter pictures demonstrate a complex history of deposition and erosion in the vicinity of the landing site (*1*). The surface within about 100 km of the landing site is characterized by sharply incised cracks that divide the terrain into polygons 5 to 10 km wide. These have been interpreted as cooling fractures in lava or, alternatively, as patterned ground produced by thermal contraction and expansion in a permafrost environment (*1*). Traced to the north, the relief of the fractured terrain becomes more subdued. On the basis of Mariner 9 pictures, it has been suggested that a mantle of aeolian debris extends equatorward from the poles to approximately 35°N (*2*). Along the margins of the mantle, several successive periods of deposition and stripping are recorded. From orbit, the surface around the site is dotted with numerous pedestal craters, an observation indicating different rates of deflation for crater ejecta and intercrater material. Ejecta deposits, probably because of an abundance of coarse-grained rubble, are more resistant to aeolian erosion. The site also contains mounds and mesas several kilometers across, which may be outliers of incompletely stripped aeolian strata.

The lander touched down about 200 km to the southwest of the 100-km crater Mie. Orbiter pictures show that a tongue of Mie ejecta extends to within a few kilometers of the most probable lander location. In fact, it is possible that the spacecraft actually landed on a more subdued distal part of the ejecta blanket.

Fluvial-like channels are visible approximately 300 km south of the landing site. The conjectured direction of flow is from east to west. However, no unequivocally fluvial features are identifiable in the immediate vicinity of the landing site.

*The first picture*. The initial sequence of images was acquired in exactly the same way as for lander 1 (*3*). Acquisition of the first picture (Fig. 1), taken by camera 2, began 25 seconds after touchdown. It covers 67.5° in azimuth and extends from 40° to 60° below a plane passing through the deck of the lander. The frame covers about 2 m² of the martian surface. The top and bottom are about 2.5 and 1.7 m from the camera, respectively. The angular resolution is 0.04°, which results in a picture element (pixel) size of 1.3 mm at a range of 1.9 m (*4*).

The bright vertical streaking on the left edge of the frame is probably the result of dust settling out of the atmosphere after being entrained by the retrorocket exhaust. The same pattern is observed in the initial Viking lander 1 image, although the dark streaking evident on the equivalent lander 1 image is missing. The streaking persists for 66 seconds in the lander 1 image and for 40 seconds in the lander 2 image (*3*).

Footpad 3 is visible in the lower right part of the frame. Just as for lander 1, fine-grained material accumulated in the concave upper surface of the footpad during descent maneuvers. Unlike the case for lander 1, clods of sediment adhered to the upper part of the sloping surface.

The footpad appears to be resting on two rocks. The surface at the extreme right side of the picture may have been broken into platy fragments, which would indicate the presence of a crust in the upper zone of the regolith. Exposed crust is visible in the lower left corner of the picture. Many of the fragments throughout the frame have platy shapes.

The larger rocks visible in Fig. 1 are much more pitted than those in the corresponding lander 1 image (*3*). The pits are probably vesicles in volcanic rocks, or, alternatively, they may be results of aeolian abrasion of rocks of varying friability. The rock just to the left of the footpad along the bottom edge of the picture displays flutes, probably the result of aeolian modification of vesicles.

*High-resolution panorama*. High-resolution images, which have been computer mosaicked, are shown in Fig. 2. Pictures were taken in the late martian afternoon (approximately 17:30 local lander time) when the sun was about 25° above the horizon. The mosaics have been geometrically rectified to compensate for lander tilt (*5*).

The surface is littered with blocks (as

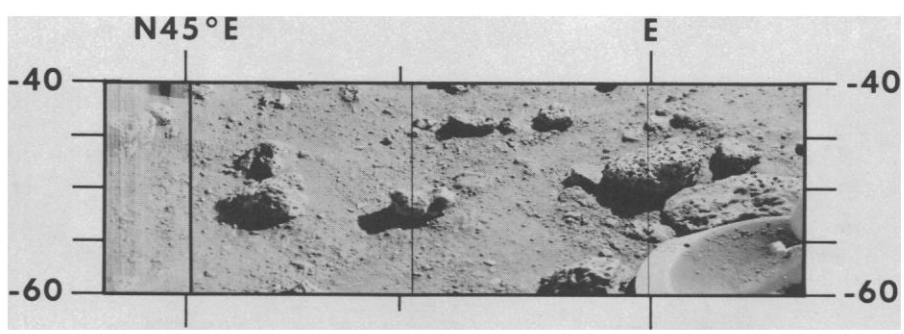


Fig. 1. This high-resolution image of footpad 3 and the adjacent surface is the first image to be returned by lander 2. Dark vertical bands are the result of temporary data loss during transmission. The image was taken in midmorning, with a sun angle of 51° above the horizon. The rock just at the top of the footpad is about 35 cm across. It appears to have been scraped or overturned during landing. The bright vertical streaks on the left of the image are probably caused by dust entrained in the atmosphere by retrorocket exhaust during landing. Most of the rocks have pits reminiscent of vesicles. Interrock areas are covered with fines that seem to be bound in a crust. Breakup of the crust probably leads to the tabular or pebbly appearance.

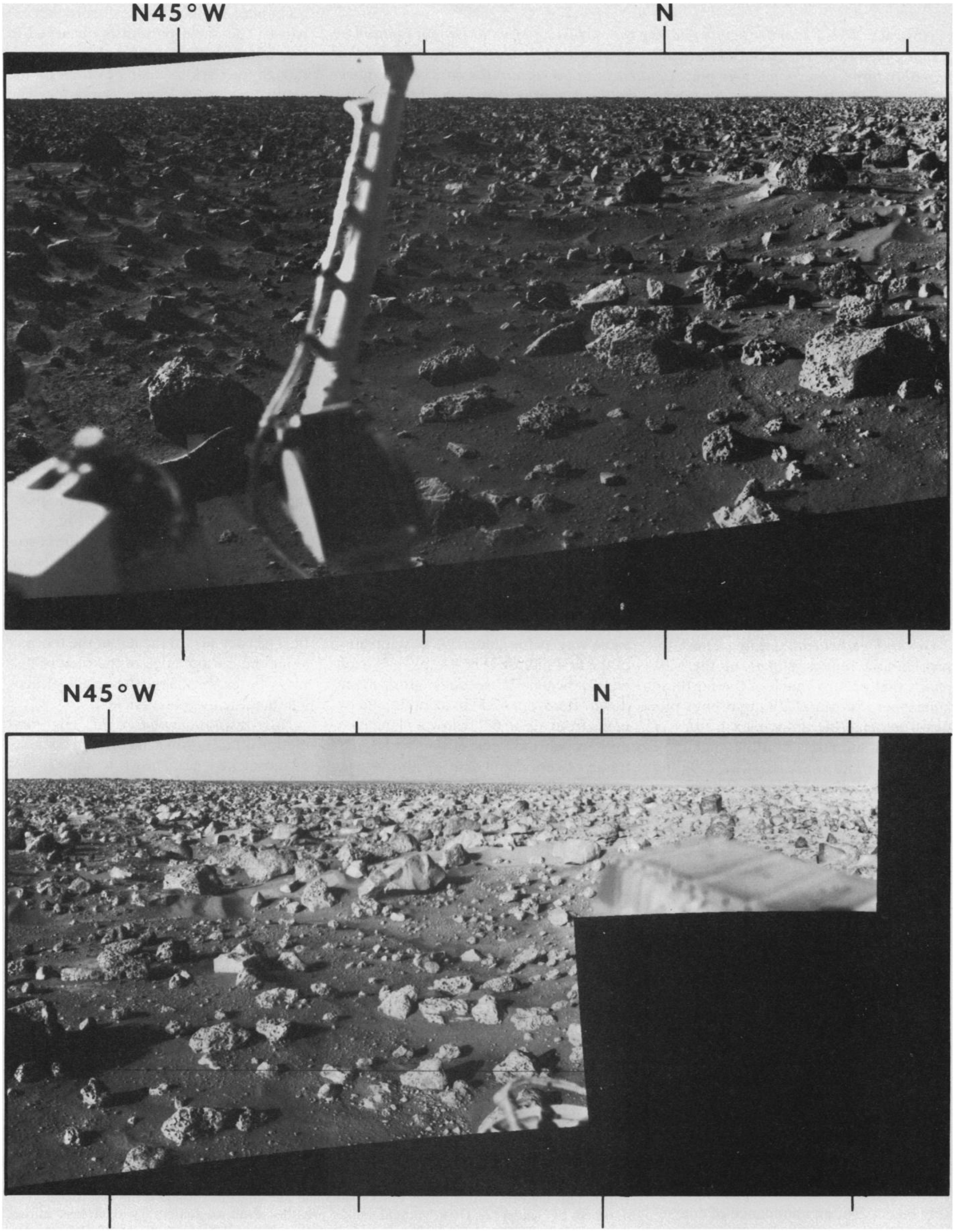


Fig. 2. Computer-generated mosaics covering most of the region seen by cameras 1 and 2 at the Viking 2 lander site are displayed as stereo pairs. Camera 1 images are on the left and camera 2 images are on the right. Geologic sketch maps for these images are shown in Fig. 3. Most of the images comprising these mosaics were acquired during the martian afternoon, with a sun angle of about 25° above the horizon. Arrows in the lower right frame point to rocks that are shown as enlargements in Fig. 4. The vertical white structure prominent on the camera 1 top image is the meteorology boom. The boxlike structure on the camera 2 images is part of the surface sampler mechanism. A bright plateau can be seen to the

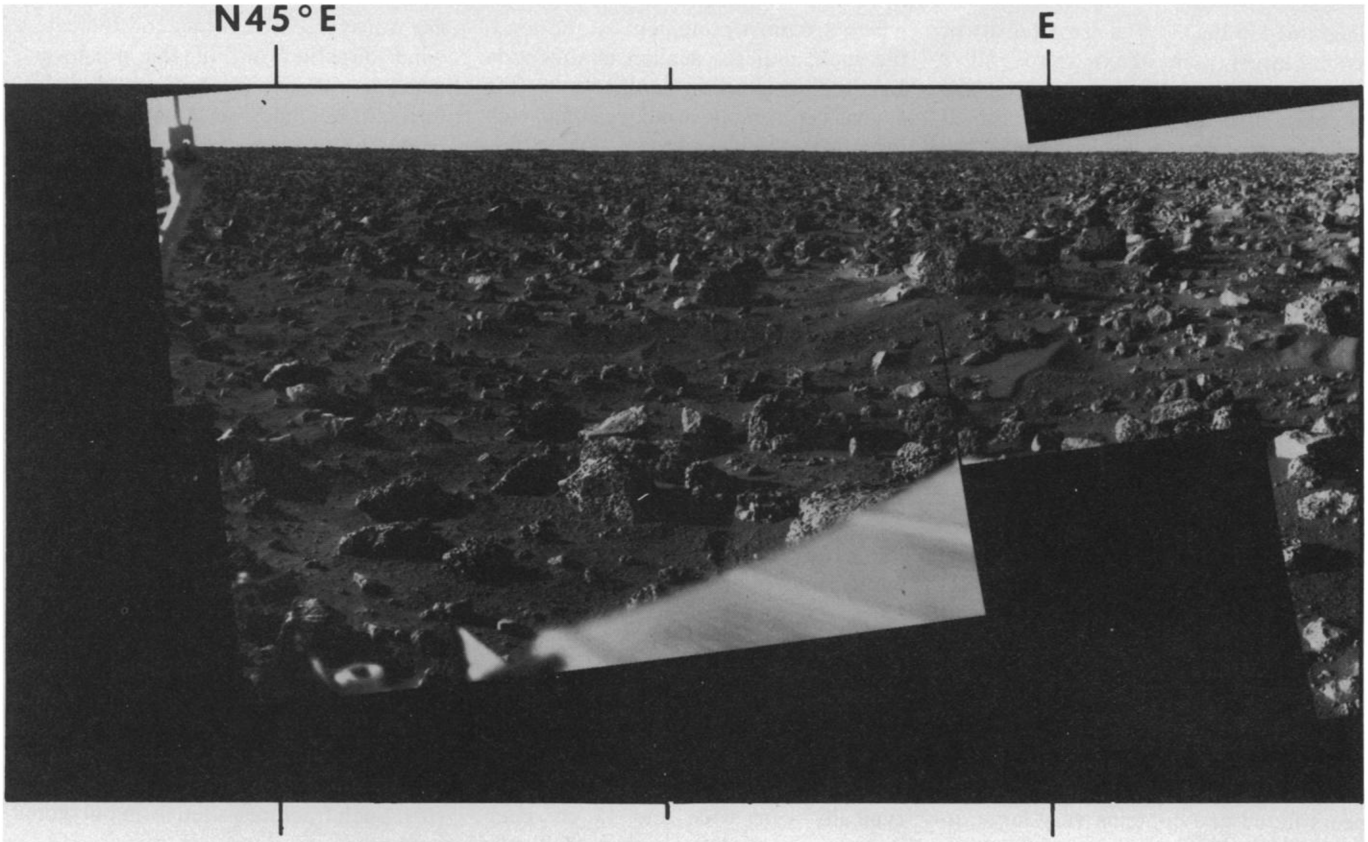


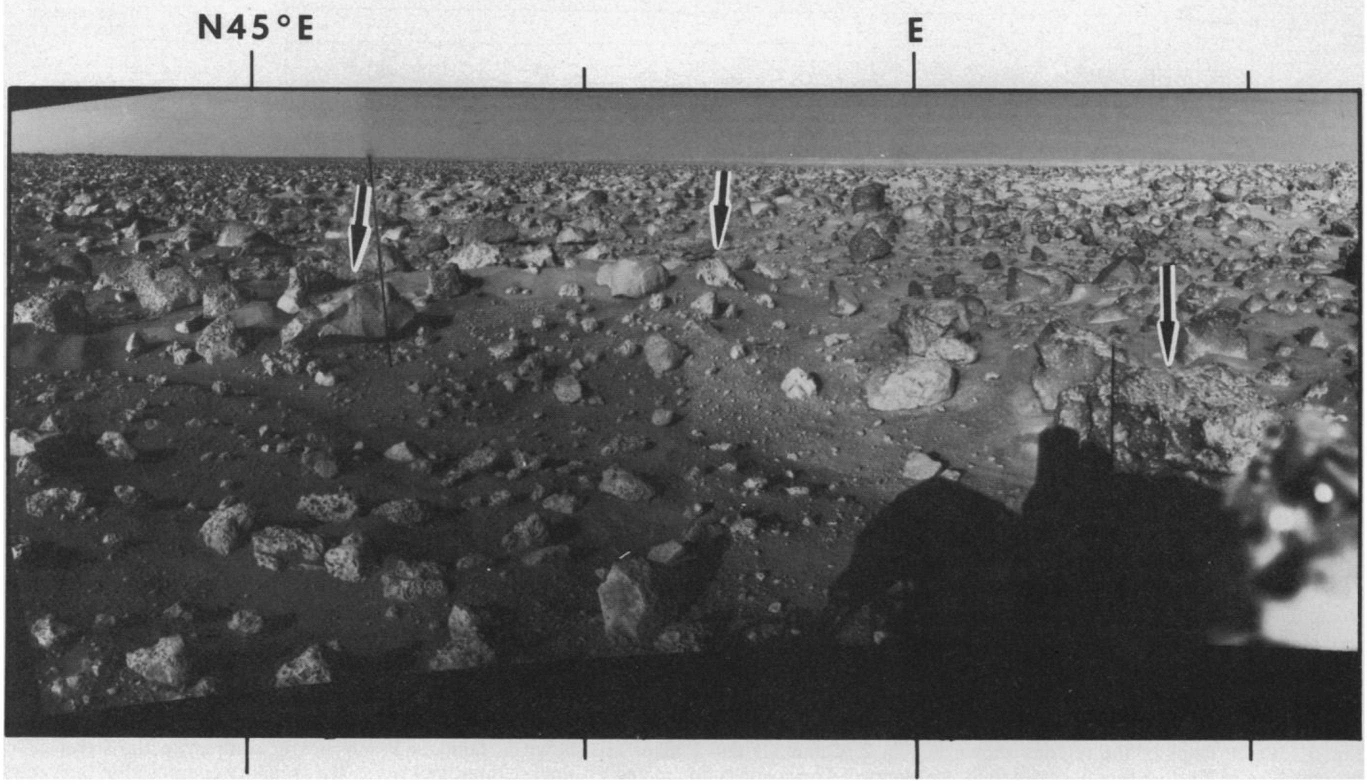


east of the spacecraft. The scene is a flat, boulder-strewn landscape. Blocks appear to be highly vesicular. Interblock regions appear to be composed of fines that are mostly bound in a coherent crust that breaks into platy fragments. A prominent trough occupies the midfield of all images. Small (10 cm high) drifts occupy the floor of the trough. For scale, the block at approximately N45°E (arrow) in the lower right frame is 1 m in width. In the midfield of the camera 1 image, at azimuth N40°W, is a smooth, bright rock, that appears to have been orthogonally fractured.

diagramed in Fig. 3). The areal density of blocks larger than 10 cm is roughly 2 times higher than that near lander 1 (*6*). In contrast to the lander 1 site, no bedrock outcrops can be discerned. The horizon is remarkably flat. Several flat-topped bluffs appear to the east of the spacecraft. The prominences correspond approximately in direction to the edge of the Mie ejecta tongue, which displays considerable relief in orbiter pictures. No evidence of the dune forms thought to be seen from orbit can be discerned from the lander imagery in Utopia Planitia.

Blocks at the lander 2 site exhibit limited diversity in texture and albedo. One particularly instructive block is conchoidally fractured and smooth on one side and pitted on the other side (Fig. 4a). At least four bands, defined in part by variable pitting, can be identified. These observations suggest that this block may have come from the top of a volcanic flow, with the vesicular part of the rock solidifying at the top.

Another vesicular rock (Fig. 4b) appears fluted and contains very large, irregular pits. The low albedo and vesicular character of the rock may indicate a volcanic origin. However, the flutes, which are most prominent on the top of the rock, indicate aeolian modification. Layered structure in another rock (Fig. 4c) has been emphasized by aeolian etching. The layering may be due to flow banding in a lava flow. Alternatively, the rock may be a welded ash. Fluvial or aeolian depositional processes cannot be ruled out, but definitive evidence is lacking.

Although a volcanic explanation for the vesicular character of the rocks is strongly suggested by terrestrial analogy, there are several alternative possibilities. If the rocks were originally massive but heterogeneous with respect to crystals or clasts, differential aeolian erosion may have etched out the softer parts of the rock. Finally, accumulation of iron oxides and hydroxides in concretional layers in terrestrial lateritic soils produces a "ferricrete" rock (*7*). Examples of this rock type are surficially similar to vesicular volcanic rocks.

Among the more provocative features at the lander 2 site are a series of intersecting troughs (Fig. 5). The troughs are typically 1 m wide and 15 cm deep, and they are relatively free of blocks. Small drifts occupy the floor of the trough in front of the lander. The drifts are transverse bed forms and indicate a wind direction out of the northwest. Analysis of fine-grained material [referred to as "fines" (*8*)] and drifts at the lander 1 site suggested that the material is composed primarily of $\leq$ 100-$\mu$m particles (*8*). If the same conclusion holds for lander 2, then the drifts are probably not sand ripples, but rather drifts of loess-sized material that somehow were able to develop a ripple-like regularity, perhaps because of the relative smoothness of the trench floor. Also, analysis of the physics of aeolian transport indicates that, because of high threshold wind velocities and low gravitational acceleration, sand ripple wavelengths should be much larger than the observed spacing between the drifts on the trench floor (*9*).

There are at least four processes that could account for trough formation. The first is cooling of lava to form contraction fractures, which typically are polygonal. A basaltic magma, upon solidification and cooling, typically undergoes a thermal contraction of large enough magnitude to generate contraction fractures (*10*). Such fractures often form polygonal networks.

A second mechanism is thermal expansion and contraction of frozen ground,

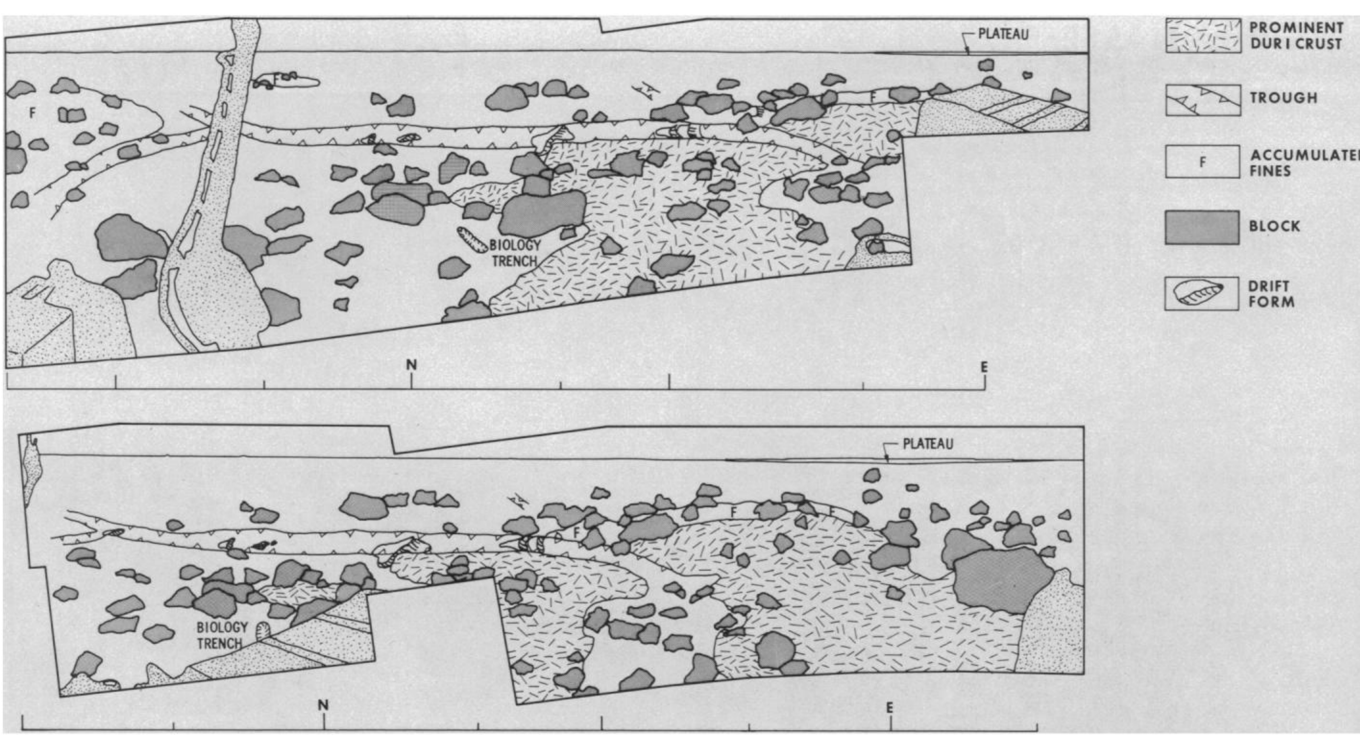


Fig. 3. Sketch maps of the regions shown in Fig. 2. Camera 1 and 2 maps are shown as contiguous mosaics in contrast to the stereo pair presentation in Fig. 2. Several terrain units are mapped. The scene is dominated by blocks. Interblock areas are primarily composed of fines that are bound in a discontinuous crust, which is broken into pebbly fragments over much of the area. Where such a crust seems dominant, it has been mapped as duricrust. Minor discrepancies exist between the two sketches because changes in viewing angle affect the appearance of the surface. Small drifts occupy the floor of the prominent trough running through the midfield of both sketches. Larger accumulations of fine material appear in the mid- to farfield (see also Fig. 2). These accumulations appear to partially bury some blocks while other blocks rest on top of the accumulations. For scale, the biology trench shown on the sketches is 40 cm in length and 8 cm wide. Spacecraft components are indicated by a light stippled pattern.

possibly accompanied by some melting. Thermal stresses, generated in ground ice because of low temperatures and rapid cooling, can also produce contraction fractures (*11*). In the terrestrial case, melting of ice during spring and summer leads to accumulation of water in contraction cracks. The water then freezes to form an ice wedge. Repetition of this annual cycle leads to growth of the fractured zone and formation of polygonally patterned ground. At the latitude of the landing site, present ground temperatures never reach values high enough to permit melting of ice (*12*). However, the cracks could have been initiated by thermal fracturing and then filled with aeolian material. If former climates were warmer, the ice wedges could have formed in a more conventional manner.

A third mechanism for polygonal fracturing is desiccation of water-saturated clay minerals. X-ray fluorescence results from both lander 1 and 2 suggest the presence of clay minerals (*13*). The pedestal craters and generally muted appearance of the lander 2 area, as viewed from orbit, suggest a considerable thickness of fine-grained material. If the fines are dominated by clays, and if they were deposited with substantial water content, then subsequent dehydration could have led to contraction and fracturing. Large dessication polygons have been identified in terrestrial playas, where they reach up to 300 m in width (*14*). Shrinkage of about 20 percent in linear dimension is observed when water-saturated montmorillonite is dehydrated (*15*).

The edges of the troughs have lips, an occurrence that is common to both desiccation and to freeze-thaw structures on Earth (*11, 14*). Since the troughs are relatively rock-free, the rocks were probably emplaced before trough formation began. Such a stratigraphic sequence is

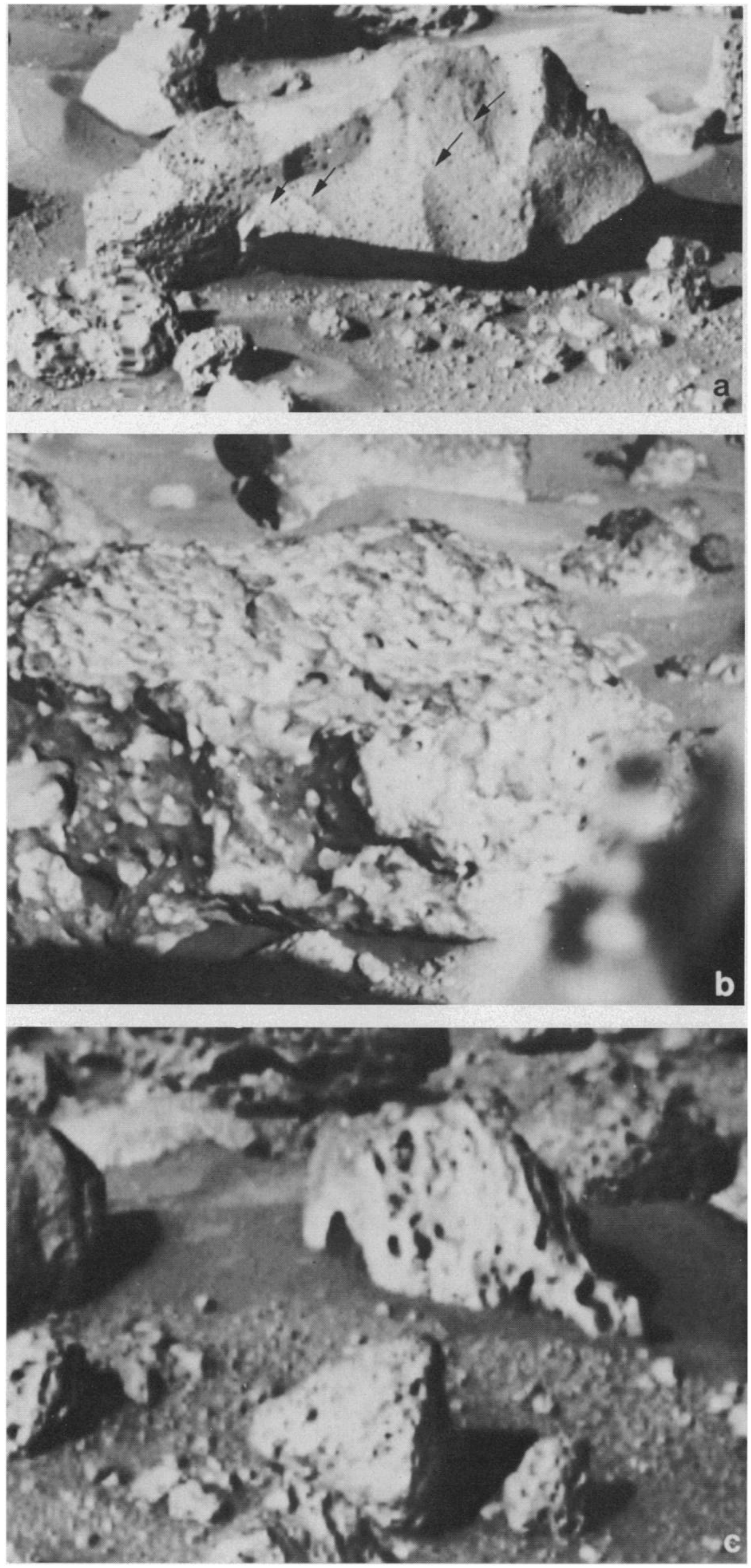


Fig. 4. Enlargements of three rocks shown in Fig. 2 have been computer-processed to show fine detail. Figure 4a shows a rock 1 m wide that is smooth on one side and pitted or vesicular on the other. The vertical band with horizontal stripping, centered at the left edge of the rock, is the result of temporary data transmission loss. Arrows point to possible banding. The appearance of both rocks is consistent with a volcanic origin. Figure 4b shows a rock near the spacecraft that is about 60 cm in width. This rock, which was imaged with a phase angle close to 0°, shows a number of pits that are probably vesicles. Figure 4c shows a rock, approximately 30 cm across, with a number of vertical bands that are probably layers. Such striae could either arise as flow bands in lava or as depositional layers, either as ash or in a more classical sedimentary environment.

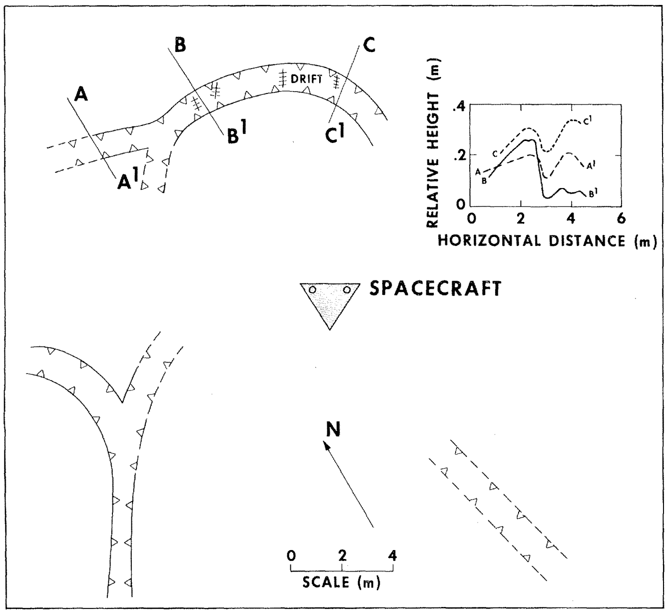


Fig. 5. Planimetric sketch map of troughs that can be seen from the lander cameras. Abrupt terminations of trough segments close to the spacecraft result because of obscuration of the surface by the spacecraft. Cross sections through selected segments of the trough are shown as an inset at upper right. The edges of the troughs appear to have lips, an occurrence that is common to terrestrial desiccation polygons and freeze-thaw polygons (*11, 14*). The position of the trough shown at lower right was derived from monoscopic ranging. Other troughs were measured by stereo ranging. Ranging errors are similar to those quoted in Mutch *et al.* (*8*).

consistent with a contraction mode of origin, since the volume created by the contraction fractures would have probably been occupied by fine-grained windblown debris. The rock-strewn surface would have had to undergo only a slight net decrease in area.

It is conceivable that the troughs have a fluvial origin. However, (i) the absence of a unidirectional pattern or topographic gradient to the troughs (Fig. 5) and (ii) the absence of recognizable fluvial bed forms (sand or gravel bars, channel bottom ripples, and so forth) argue against fluvial processes. In addition, it is difficult to envision how a given fluid would be capable of carving only small (1 m wide), shallow channels and yet be able to remove blocks comparable in size to the channel dimension.

The polygonal pattern of fractures persists to the centimeter scale. Many of the observed pebbles at both lander 1 and 2 sites seem to be angular fragments of duricrust. Duricrust is used here as a descriptive term that refers to indurated fine-grained material with a nonzero tensile strength. It may be formed by desiccation of clay minerals and concentration of salts by evaporation of volatiles in the upper few centimeters of the regolith. In several areas, unfractured duricrust can be traced through polygonally fractured slabs to pebbly regions (Fig. 2).

*Lander 1 and 2 sites compared.* Since both landing sites were chosen, for reasons of safety, for their topographic blandness, it cannot be directly concluded that the small-scale features seen by the lander cameras are typical of similar features elsewhere on Mars. Indeed, the view from the Viking orbiters suggests an exuberance of geologic diversity. At first glance, both lander 1 and 2 sites appear to be similar block-strewn landscapes. However, there are a number of differences in detail. The lander 2 site is generally flat. Bedrock is exposed at the first site but not at the second. Large drifts are observed at the first site but not at the second. Polygonal troughs are at the second site but not at the first. Lander 1 rocks display a great deal of diversity in albedo, shape, and texture, whereas lander 2 rocks are almost all similar in albedo and vesicular texture. Although aeolian stripping is better revealed at the lander 2 site, individual boulders show more prominent evidence of wind faceting at the lander 1 site. No changes to the surface other than those due to sampling activity have been detected at either site. This is consistent with the low wind velocities at both sites: the wind speeds so far have been below the threshold for particle movement. As with lander 1 (*3*), no evidence, direct or indirect, has been obtained for macroscopic biology on Mars. It must be remembered, however, that only a tiny fraction of time and space has been sampled.

*The sky at the lander 2 site.* The sky at the second lander site exhibits properties qualitatively similar to those at the first site. Thus, a number of conclusions drawn about the sky at the first site are equally valid for the second (*3, 8*). At the second site, the sky has a brightness comparable to that of the surface, and hence almost all of the sky brightness is due to scattering by particles suspended in the atmosphere, with only a negligible contribution from atmospheric Rayleigh scattering. Also, the initial color reconstructions suggest that the sky color above the second site is similar to the ground color. This result would imply that a substantial fraction of the suspended particles above the second site consists of very fine-grained soil particles that absorb preferentially in the blue. Finally, the increase of sky brightness with decreasing angular distance from the sun, at distances close to the sun, is comparable to that found at the first site. Thus, the mean atmospheric particle size is quite similar at the two sites ($\sim 1$ $\mu$m).

While the sky is qualitatively similar above the two sites, there is one important quantitative difference. Observations of the brightness of the sun at several different elevation angles imply that the optical depth of the atmosphere above the second site is approximately 0.25 at an effective wavelength of 0.67 $\mu$m. By contrast, similar measurements performed at the first landing site, on days overlapping the period of observations at the second site, lead to an optical depth of about 0.35. This difference in optical depth exceeds plausible errors in the results. Furthermore, lander 2 is at a lower elevation than lander 1, so the difference cannot be attributed to elevation differences. This comparison indicates significant regional differences in optical depths.

*Status of the Viking mission.* The primary phase of the lander 1 mission ended with transmission to Earth on 2 September 1976. The lander 1 reduced mission, during which data were recorded on tape and relayed to Earth over the direct communication system, lasted from 2 September to 5 November 1976. The lander 2 primary mission ended on 5 November 1976, just before conjunction. A total of about 450 images were acquired by lander 1 and about 575 images by lander 2. The imagery was divided among high-resolution composites, normal color composites, seven-channel spectrophotometric composites, atmospheric and surface experiments, sample support imagery, and imagery to support physical and magnetic properties experiments. With the advent of the extended mission, lander imagery experiments aimed at monitoring changes in atmospheric properties and surface features will be implemented in order to understand Mars as it varies through the seasons.

T. A. MUTCH, S. U. GRENANDER
K. L. JONES, W. PATTERSON
*Department of Geological Sciences, Brown University, Providence, Rhode Island 02912*
R. E. ARVIDSON
E. A. GUINNESS
*McDonnell Center for the Space Sciences, Department of Earth and Planetary Sciences, Washington University, St. Louis, Missouri 63130*
P. AVRIN
C. E. CARLSTON
*Martin Marietta Corporation, Denver, Colorado 80201*
A. B. BINDER
*Institut für Geophysik, University of Kiel, Federal Republic of Germany*, and *Science Applications, Inc., Pasadena, California 91101*
C. SAGAN, E. W. DUNHAM
P. L. FOX, D. C. PIERI
*Laboratory for Planetary Studies, Cornell University, Ithaca, New York 14853*
F. O. HUCK, C. W. ROWLAND
G. R. TAYLOR, S. D. WALL
*NASA Langley Research Center, Hampton, Virginia 23665*
R. KAHN
*Center for Earth and Planetary Physics, Harvard University, Cambridge, Massachusetts 02138*
E. C. LEVINTHAL, S. LIEBES, JR.
R. B. TUCKER
*Department of Genetics, School of Medicine, Stanford University, Stanford, California 94305*
E. C. MORRIS
*U.S. Geological Survey, Flagstaff, Arizona 86001*
J. B. POLLACK
*NASA Ames Research Center, Moffett Field, California 94305*
R. S. SAUNDERS, M. R. WOLF
*Jet Propulsion Laboratory, Pasadena, California 91103*

**References and Notes**

1. H. Masursky and N. L. Crabill, *Science* **194**, 62 (1976).
2. L. Soderblom, T. Kreidler, H. Masursky, *J. Geophys. Res.* **78**, 4117 (1973).
3. T. A. Mutch, A. B. Binder, F. O. Huck, E. C. Levinthal, S. Liebes, Jr., E. C. Morris, W. R. Patterson, J. B. Pollack, C. Sagan, G. R. Taylor, *Science* **193**, 791 (1976).
4. F. O. Huck, H. F. McCall, W. R. Patterson, G. R. Taylor, *Space Science Instrum.* **1**, 189 (1975).
5. In addition to corrections for lander tilt, each image was processed to remove geometric distortions related to use of high-resolution photodiodes that are located at different locations on the camera's photosensor array.
6. Block counts were made from the lander 2 sol 0 camera 2 survey image for a region extending 15 m in front of the spacecraft. More refined block counts reduced by computer processing of stereo pairs will appear in a forthcoming paper.
7. H. Blatt, G. Middleton, R. Murray, *Origin of Sedimentary Rocks* (Prentice-Hall, Englewood Cliffs, N.J., 1972).
8. T. A. Mutch, R. E. Arvidson, A. B. Binder, F. O. Huck, E. C. Levinthal, S. Liebes, Jr., E. C. Morris, D. Nummedal, J. B. Pollack, C. Sagan, *Science* **194**, 87 (1976). The 100-μm upper limit on particle size is an inference, since the pixel size on the surface at optimum focus is about 1 mm. The inference is based on (i) the mechanical behavior of material exposed in trenches [R. W. Shorthill, H. J. Moore, II, R. F. Scott, R. E. Hutton, S. Liebes, Jr., C. R. Spitzer, *Science* **194**, 91 (1976)], and (ii) the observation that at both sites the fines seem to be dominated by clay minerals (*13*), which are characteristically fine-grained.
9. C. Sagan, in preparation.
10. J. Jaeger, *Am. J. Sci.* **259**, 721 (1961).
11. A. Lachenbruch, *Geological Society of America Special Paper No. 70* (1962).
12. F. Wade and J. DeWys, *Icarus* **9**, 175 (1968).
13. A. K. Baird, P. Toulmin, B. C. Clark, H. J. Rose, Jr., K. Keil, R. P. Christian, J. L. Gooding, *Science* **194**, 1288 (1976).
14. J. Neal, A. Langer, P. Kerr. *Geol. Soc. Am. Bull.* **79**, 69 (1968).
15. R. Grim, *Applied Clay Mineralogy* (McGraw-Hill, New York, 1962).
16. A large number of people have contributed to the success of the Viking mission. In particular our thanks go to the Viking management, to the lander mission planning groups, and to the analysts at the Image Processing Laboratory at the Jet Propulsion Laboratory. We are also most grateful to the group of undergraduate students who worked on various phases of lander imagery as part of the Viking intern program, supported by the Planetology Program Office, NASA Headquarters, and by the Alfred P. Sloan Foundation. This research was supported by NASA.

15 November 1976

# Inorganic Analyses of Martian Surface Samples at the Viking Landing Sites

Abstract. *Elemental analyses of fines in the Martian regolith at two widely separated landing sites, Chryse Planitia and Utopia Planitia, produced remarkably similar results. At both sites, the uppermost regolith contains abundant Si and Fe, with significant concentrations of Mg, Al, S, Ca, and Ti. The S concentration is one to two orders of magnitude higher, and K (< 0.25 percent by weight) is at least 5 times lower than the average for the earth's crust. The trace elements Sr, Y, and possibly Zr, have been detected at concentrations near or below 100 parts per million. Pebble-sized fragments sampled at Chryse contain more S than the bulk fines, and are thought to be pieces of a sulfate-cemented duricrust.*

Each Viking lander carries an energy-dispersive x-ray fluorescence spectrometer (XRFS) for elemental analysis of samples of the martian surface. The design characteristics and expected performance capabilities for this instrument have been described elsewhere (*1*). In an earlier report, we presented preliminary results of the first analysis of fines in situ at Chryse Planitia (*2*). Although data collection and reduction are still in progress, we present in Tables 1 and 2 our interim results of the analyses accomplished to date.

*Analysis methods.* Because of the weight constraints on the Viking pay-

Table 1. Element abundances in Mars samples. Concentrations are expressed as percentages by weight. NA indicates that data are not yet available.

| Element | S1 | S2 minus S1 | S3 minus S1* | U1 minus S1 |
|---|---|---|---|---|
| Mg | 5.0 ± 2.5 | NA | +0.2 | NA |
| Al | 3.0 ± 0.9 | NA | −0.1 | NA |
| Si | 20.9 ± 2.5 | −0.1 | −0.4 | −0.9 |
| S | 3.1 ± 0.5 | +0.7 | +0.7 | −0.5 |
| Cl | 0.7 ± 0.3 | +0.1 | +0.2 | −0.1 |
| K | <0.25 | 0 | 0 | 0 |
| Ca | 4.0 ± 0.8 | −0.2 | 0 | −0.4 |
| Ti | 0.51 ± 0.2 | 0 | 0 | +0.1 |
| Fe | 12.7 ± 2.0 | −0.1 | +0.4* | +1.5 |
| "O"† | 50.1 ± 4.3 | NA | NA | NA |
| X† | 8.4 ± 7.8 | NA | NA | NA |

*All S3 concentrations have been adjusted by a preliminary correction factor of 0.9 to compensate the effect of a partial fill on the analysis. The Fe is also affected by the contribution of $^{55}$Fe to the peak. Trace elements analyze low. †"Oxygen" is the sum of all elements not directly determined. If the detected elements are all present as their common oxides (Cl excepted), then $X$ is the sum of nondetected components, including $H_2O$, $Na_2O$, $CO_2$, and $NO_x$.